Supporting Information

Gonzalez-Bellido et al. 10.1073/pnas.1014438108

SI Materials and Methods

Transmission and Scanning EM. The dissection and fixation protocols for EM were as previously described (1, 2). Fly heads were dissected under a drop of 2.5% glutaraldehyde, 2.5% paraformaldehyde in 0.1 M sodium cacodylate/HCL buffer (pH 7.3) and then fixed in the same solution for 2 h at room temperature. After washing in cacodylate buffer, the samples were placed in 1% osmium tetroxide in veronal acetate for 2 h at 4 °C. After further washing, the samples were dehydrated for 7 min in alcohol in each of the following concentrations: 50%, 70%, 80%, 90%, 95%, and 100%. The dehydration with 100% ethanol was repeated two times. For the last change, the ethanol used had been dried over anhydrous copper sulfate. Next, the samples were placed in two 10-min changes of propylene oxide (PPO). For embedding, the specimens were placed in a 50/50 mix of PPO and Epon resin (Poly/Bed 812, Polysciences) overnight. The next day, the specimens were put into several changes of fresh resin and placed in an oven at 60 °C for 12 h. Serial 60-nm sections were stained with uranyl acetate and lead citrate and examined at 80 kV in a Philips Tecnai 12 electron microscope. Images were captured with either an Orius 1000 or a Gatan Model 791, cooled MultiScan wide-angle CCD camera (side-mounted; 1,024 × 1,024 pixels).

For scanning EM, the samples were processed as for transmission EM, but after alcohol dehydration they were placed in a 50/50 mix of alcohol and hexamethyldisilazane for 30 min and then transferred to 100% hexamethyldisilazane for a further 30 min. Subsequently, the samples were allowed to air-dry overnight. The next day the samples were mounted on stubs, gold coated in an Edwards S150B sputter coater, and viewed with a Philips XL-20 scanning electron microscope.

Our tissue was not corrected for shrinkage. To prevent shrinkage, our samples were transferred through a series of ethanol steps slowly. The resin selected for this study, Polybed 812, has low shrinkage. Moreover, two previous studies that used a similar protocol for processing of transmission EM samples (including Polybed 812) reported either no shrinkage (3) or 4.3% shrinkage (4). Thus, it is conceivable that the transmission EM measurements area is up to 5% larger in live animals. These numbers serve only as an approximation, because shrinkage is tissue-type dependent. For instance, small dipteran heads have a relatively large area of cuticle, which helps reduce tissue deformation. Both species were processed at the same time, so tissue shrinkage should be equivalent.

Lens Diameter. High-magnification scanning EM images (800× or 1,000×) were taken at different locations over the whole left eye of each specimen studied. Care was taken such that no images overlapped. The specimen was rotated so that the ommatidial axis was always perpendicular to the camera. The diameter of the lenses was measured from each photographed location, with ImageJ software (National Institutes of Health), as the distance from the center of a lens to the center of the neighboring lens, either four (square array) or six (hexagonal array) neighbors, depending on the ommatidia arrangement. The mean diameter was then calculated for the center lens. For each photographed location, five "center" lenses, with nonoverlapping measurements, were chosen and their mean obtained (Fig. S4*C*). The mean for each location has been plotted in Fig. 2*A* (main text) according to their coordinates on the eye, which were estimated visually from low-magnification images. Because of preparation damage, most of the posterior part of the male *Coenosia* eye was deemed not suitable for analysis.

Rhabdomere Diameter. Transmission EM images were taken at two levels in the retina: below the rhabdomere caps and more proximally. At least 12 ommatidia ($n \geq 12$) were used to calculate mean and SEM for each ommatidium level and specimen studied. The images were processed with ImageJ software. Rhabdomeres better approximate an ellipse shape, not a circular one (5). Hence for maximum precision, the rhabdomere area was selected manually, fitted with an ellipse (Fig. S4*D*), and its major and minor diameters were then recorded.

Rhabdomere Width Limit and Waveguide Properties. If the wavelength of light is similar to the width of the structure along which it travels, the light is not distributed evenly (6), and stable patterns of light excitation distribution, called waveguide modes, are formed (5, 7). The narrower the waveguide (rhabdomere), the lower number of modes it propagates (5). In addition, narrower waveguides propagate a higher proportion of light outside their boundary, where photons will not hit rhodopsin pigments. However, the shorter the light wavelength, the larger the proportion of light propagated within the waveguide (8). Thus, for efficient light capture, there is likely a selection pressure to use short-wavelength absorption pigments in thin rhabdomeres. This also implies that for a given wavelength there is a practical limit to the width of the rhabdomere. Horridge et al. (9) estimated that for fly rhabdomeres this limit is 0.7 μm, which is the R7/R8 major rhabdomere width of killer flies. Because the R1–R6 rhodopsin has a longer absorption peak, it is possible that the width of these rhabdomeres has also hit the practical limit.

Mitochondria and Photoreceptor Cytosol Areas. Transmission EM images were taken at the same level in the retina; just below the interface of R7 and R8. From 10 ommatidia for each species, the cytosol and mitochondria profiles of photoreceptors R1–R6 were hand traced in ImageJ (Fig. S4 *A* and *B*) and the mean area and SEM calculated.

Interommatidial Angle and Light Microscopy. Semithin (0.5-μm) longitudinal sections were cut horizontally (antennae to neck; Fig. S1 *A* and *B*) and diagonally along an ommatidia row, which crossed the eye from posterior to anterior in the medial part of the eye [Fig. 2*C* (main text) and Fig. S2 *A* and *B*]. The angles from five neighboring ommatidia were averaged (±SEM).

For light microscopy, tissues were prepared as described for the transmission EM sections. Semithin sections of 0.2- to 0.5-μm thickness were obtained and stained with 1% Toluidine Blue dissolved in 1% Borax. The samples were viewed and photographed with a ScanScope GL scanner (Aperio Technologies).

Focal Length. Focal length was measured experimentally as previously described (10, 11). Briefly, the whole cornea was carefully cut away and the photoreceptors removed with a brush. The cornea was suspended on a drop of fly saline placed on a coverslip. The preparation was inverted and dropped onto an O ring with Vaseline, which sealed the preparation. The preparation was viewed with an Olympus SZX12 stereo microscope with a 1× Dark Field Plan Apochromat (DF PLAPO) objective and an AL-20× objective extension. Maximum zoom was used, which equated to 90×. The image formed by the lens (Fig. S4*E*) was captured through a 2× adaptor followed by a JCV color video camera (TK-C1481 BEG). Two *Coenosia* ($n = 2$) and one

Drosophila (n = 1) corneas were dissected from female specimens. The focal length was measured for all lenses ($n \geq 14$) in the lateral region of the eye, whose axis was assessed to be perpendicular to the image. The mean ± SEM was calculated for *Coenosia* from representative values of each cornea (n = 2). For *Drosophila*, a representative mean value from one cornea is reported. To calculate the focal length (f), Eq. **S1**, from Somanathan et al. (12), was applied.

$$f = s_o \frac{\lambda_i}{\lambda_o} \quad \textbf{[S1]}$$

where s_o = distance between lens and object, λ_o = spatial wavelength of the object pattern, and λ_i = spatial wavelength of the image pattern (12).

Estimating Focal Length by Cornea Drop Method. The observations yield f = 21.36 μm (n = 1) for *Drosophila* and f = 24.70 μm ± 1.15 SEM (n = 2) for *Coenosia* (Table S1) in the lateral eye. The f value obtained for *Drosophila* is comparable to the previous histological estimates of f = 20 ± 2 μm [see ref. (7)]. Although shortage in samples prevented us from affirming the focal length in other areas of the *Coenosia* eye, in cross-section, the increase in the pseudocone length (compare Fig. S1*A*) in the frontal area indicated an increase in focal length.

Calculating Cross-Talk Index. To calculate the *cross-talk index*, Eq. **S2**, from Wijngaard and Stavenga (13), was applied.

$$\text{Cross-talk index} = (e/b) + 2 \quad \textbf{[S2]}$$

where e is the space between the boundaries of the rhabdomeres, and b is the radius of the rhabdomere.

Intracellular Recordings. We recorded intracellularly from R1–R6 photoreceptors in the retina of fruit flies and killer flies at 19 °C with sharp quartz microelectrodes (typical resistance: 120–220 MΩ with 3 M KCl) pulled on a Sutter Instruments P2000 electrode puller. Briefly, a reference electrode, placed inside the head capsule through the ocelli, was filled with fly ringer (Fig. S3*J*). A hole of ≈4 × 4 ommatidia was cut on the cuticle of the left eye (Fig. S3*K*) to allow insertion of a sharp quartz electrode. A high-power light-emitting diode (Seoul Z-Power LED P4 star, white, 100 lumens) was fitted with a lens and a metal plate with a pinhole in front of the light-emitting diode (LED) to narrow the subtended angle to 0.7°. The whole LED unit was installed onto on a Cardan arm system and was driven by an OptoLED (Cairn Research), which has optical feedback to maintain stable light output even if the LED temperature changes. The turntable (X position) and the cardan arm (Y position) were motorized such that the LED could be controlled on X and Y coordinates by remote control. The intensity of the light output was calibrated by matching the voltage given by the OptoLED driver to calibrated neutral density filters (Stouffer) so that the intensity of the light output could be controlled remotely with BIOSYST, a custom-built MATLAB interface (14, 15). To scale the intensity range of the LED further than its practical operational limit, a wheel of neutral-density filters was placed in front of the pinhole. The center of a cell was located by using low light intensity and moving the LED until the maximum response (mV) was obtained. Only cells with a resting potential below −60 mV were selected for this study. Data were sampled at 1 to 2 kHz with a National Instruments 12-bit A/D converter and analyzed offline with BIOSYST.

Voltage/Log[Intensity] Relationship. V/LogI curve was obtained, after locating the axis of the impaled cell, by increasing the light intensity in steps of 0.25 log units for the full range of the LED. This was repeated with and without neutral-density filters. The maximum voltage response obtained from each light intensity pulse was fitted with a sigmoid Hill function, shown in Eq. **S3**.

$$\widehat{V} = A^* \frac{\left(\frac{I}{I_{50}}\right)^n}{1 + \left(\frac{I}{I_{50}}\right)^n} \quad \textbf{[S3]}$$

where $\widehat{V}$ = estimated voltage values; A^* = amplitude; I = LogI; and I_{50} = LogI at 50% of the maximum voltage response. To obtain the Hill coefficient (n), a nonlinear fitting routine in MATLAB, called "nlinfit," was applied.

Angular Sensitivity. The light intensity was chosen to elicit a 50–75% of the maximum voltage response when on-axis. The LED was displaced vertically, lowering its position between 5° and 15°, and then moved upwards in steps of 0.5° for a total of 30° for *Drosophila* and 10° for *Coenosia*. The elapsed time in darkness from each vertical position to the next was ≈7 s. The stimulus at each vertical step consisted of two light pulses of 10-ms duration, separated by 1.2 s of darkness. The average maximum voltage for each location was recorded and converted to sensitivity by using the V/LogI curve and Eq. **S4**. The resulting angular sensitivity curve was fitted with a Gaussian whose half-width was recorded. The MATLAB scripts (by Uwe Friederich and Zhuoyi Song) were used for fitting the Hill sigmoid, obtaining sensitivity values, and fitting Gaussians.

$$\text{Sensitivity \% at step (n)} = 100^* 10^{\log[Intensity_{V\max} - Intensity_{Vn}]} \quad \textbf{[S4]}$$

where $Intensity_{V\max}$ = corresponding log light intensity (in the Voltage/LogI curve), for the maximum voltage change obtained. $Intensity_{Vn}$ = corresponding log light intensity (in the Voltage/LogI curve) for the voltage change obtained at "n" position.

The intracellularly measured acceptance angles of *Drosophila* photoreceptors are twice as large as the previous behavioral and theoretical estimates: 3.5° (16) and 4.2° (7), respectively, which are actually much closer to the values of *Coenosia* photoreceptors. To some extent these differences may be accounted for the light-adapted conditions of the behavioral experiments, in which the receptive fields of the dipteran flies are known to narrow by ≈20%, owing to intracellular pupil and screening pigment movements (17). Nonetheless, large acceptance angles that deviate strongly from predictions are sometimes explained by mechanical damage to the optics of the eye (18). This is unlikely here, because we could remove very small pieces of cornea from the *Drosophila* eye with little injury to the underlying retina (Fig. S3 *K* and *L*), leaving the microelectrode impalement as the only possible impairment. Even then, recordings obtained from cells with damaged optics show asymmetrical angular sensitivity curves (18). This was not the case for any of the cells in this study. Therefore, the Δρ values that we report for nearly dark-adapted *Drosophila* are unlikely to be influenced by experimental artifacts, and they should provide a realistic account of photoreceptor acuity in dim conditions.

Latency Measurements. Briefly dark-adapted R1–R6 photoreceptors (1 to 2 min) were stimulated with a bright 10-ms light pulse, evoking saturated voltage responses [Fig. 3*B* and Fig. S3*A* (main text)]. We selected low-noise responses of similar amplitudes (*Drosophila*: 47.6 ± 5.2 mV, n = 5; *Coenosia*: 45.7 ± 3.4 mV, n = 18; *Calliphora*: 48.6 ± 3.2 mV, n = 5; mean ± SD) and measured their latencies. Here, latency was defined as the time from the stimulus onset to a clear "up-notch" in the first derivative of their responses (Fig. S3*B*). This endpoint was taken to indicate when the light-gated conductances, through the mass-opening of the trp/trpl-channels (19), begin to charge the plasma membrane.

Because the recordings had practically flat first-derivatives until the "up-notch," such measurements were unambiguous.

We expect that our latency estimates (*Coenosia*: 2.8 ± 0.5 ms; *Calliphora*: 5.4 ± 0.5 ms; *Drosophila*: 6.2 ± 0.8 ms; mean ± SD) assert reliably the quickness of the underlying phototransduction reactions, being unbiased by membrane filtering, because:

i) Patch-clamp experiments, which measure directly the speed of phototransduction cascade in dissociated R1–R6 *Drosophila* photoreceptors, give identical latency estimates (≈6 ms) for the onset of the light-gated conductances after a bright light pulse (19).

ii) The estimated latencies of dark-adapted *Calliphora* and *Drosophila* photoreceptors are very similar, even though their membrane time constants vary fivefold (*Drosophila*: $\tau \approx 20$ ms; *Calliphora*: $\tau \approx 4$ ms) and input impedances 10-fold (*Drosophila*: $R_i > 300$ MΩ; *Calliphora*: $R_i = 32$ MΩ) owing to different membrane areas and ion-channel compositions (15, 20). Nonetheless, their similar latencies are unsurprising. Their membrane bandwidths, even when dark-adapted, are two to five times broader than their respective transduction cascades; thus, in real terms, the plasma membrane does not limit notably the speed of the phototransduction signal while filtering off high-frequency noise (15, 21, 22).

iii) The *Coenosia* photoreceptor membrane is that of a fast photoreceptor (Fig. S3C), having $\tau = 3.1 \pm 0.5$ ms and $R_i = 41.2 \pm 5.8$ MΩ (mean ± SD, $n = 15$). Again, these values are too close to those of *Calliphora* photoreceptors to account for the large difference in their latency estimates; in particular, because we know that τ of Calliphora membrane reduces from 4 to 1 ms (or less) when the light-gated conductances start depolarizing it (20, 22).

Linear Impulse Responses. A bright light background was turned on for 10 s, followed by repeated presentations (10–15 times) of a 10-s-long pseudorandom light contrast stimulus, $c(t)$, superimposed upon it (15). $c(t)$ was generated using MATLAB functions; it had Gaussian amplitude distribution and was approximately "flat" up to 200 Hz. It evoked similar changes in the responsiveness and information transfer of *Drosophila* and *Calliphora* photoreceptors, as reported earlier (15), without allocating much power on light patterns that are too fast for these cells to follow at 19 °C.

We calculated the transfer function $T(f)$ (Eq. **S5**) between the average voltage response, or "signal" $s(t)$, and the contrast stimuli using their 1,024-point-long spectral estimates, $S(f)$ and $C(f)$, respectively.

$$T(f) = \frac{\langle S(f) \cdot C^*(f) \rangle}{\langle C(f) \cdot C^*(f) \rangle} \qquad \textbf{[S5]}$$

Here <> denotes the average over the different stretches, and * the complex conjugate. The linear impulse response, or first-order Wiener kernel (6), was then simply obtained by taking the inverse Fourier transform of its frequency response:

$$K_1(t) = F^{-1}[T(f)] \qquad \textbf{[S6]}$$

Signal-to-Noise Ratio. One-second-long naturalistic light intensity series (10,000 points), selected from the van Hateren natural stimulus collection (23), was repeated more than 100 times, and the evoked voltage responses of a photoreceptor were recorded (Fig. S3 *D–F*). We rejected the 5–20 first traces from the analysis because they displayed systemically adaptive trends. For each recording series (Fig. S3 *G–I*), the averaged response was the "signal," whereas the "noise" was the difference between individual traces and the signal. Hence for an experiment using n trials (with $n = 50$–100) there is one signal trace and n noise traces.

For the analysis, the signal and noise traces were divided into 50% overlapping stretches and windowed with a Blackman-Harris four-term window, each giving three 500-point-long samples. Because all of the data from the 50–100 voltage traces were used, we obtained 150–300 spectral samples for the noise and three spectral samples for the signal. These were averaged, respectively, to improve the estimates.

Signal-to-noise ratio, $SNR(f)$, of the voltage responses was calculated from the signal and noise power spectra, $<|S(f)|^2>$ and $<|N(f)|^2>$, respectively, as their ratio (Fig. 4*C*, main text), where ‖ denotes the norm and <> the average over the different stretches (15).

Rate of Information Transfer. A photoreceptor's voltage responses to naturalistic stimulation, NS, are typically nonlinear and non-Gaussian (14, 23); for such conditions the classic Shannon formula for the information capacity (24) does not apply. Thus, to calculate the rate of information transmitted by the photoreceptors, we used the triple extrapolation method (14), which has been shown to obtain robust estimates from continuous neural responses (14, 21, 25, 26).

The voltage responses of the *Drosophila*, *Coenosia*, or *Calliphora* photoreceptors were first digitized by dividing it into time intervals, T, that were subdivided into smaller intervals $t = 1$ ms. This procedure selects "words" of length T with T/t "letters." The mutual information between the voltage response S and the light contrast stimulus is then the difference between the total entropy:

$$H_S = -\sum_i P_S(s_i) \log_2 P_S(s_i) \qquad \textbf{[S7]}$$

and the noise entropy:

$$H_N = -\left\langle \sum_{i=1} P_i(\tau) \log_2 P_i(\tau) \right\rangle_\tau \qquad \textbf{[S8]}$$

where $P_i(\tau)$ is the probability of finding the ith word at a time t after the initiation of the trial. This probability $P_i(\tau)$ was calculated across trials of identical NS. The values of the digitized entropies depend on the length of the words T, the number of voltage levels v, and the *size* of the data file, $H^{T,n,size}$. The rate of information transfer was then obtained taking the following three successive limits:

$$R = R_S - R_N = \lim_{T\to\infty} \frac{1}{T} \lim_{v\to\infty} \lim_{size\to\infty} \left(H_S^{T,v,size} - H_N^{T,v,size} \right) \qquad \textbf{[S9]}$$

These limits were calculated by extrapolating the values of the experimentally obtained entropies. Because after removing the first trial (the first 5–20 traces when an adaptational trend could be seen), we typically used the next 100 traces (1-kHz sampling rate), thereby having a response matrix of 1,000 points × 100 trials for the analysis. The total entropy and noise entropy were then obtained from the response matrices using linear extrapolation with the following parameters:

size = 5/10, 6/10,. . .,10/10 of data; n = 6, 7,. . .,11 voltage levels; T^{-1} = 3, 4,. . .,6 points.

1. Meinertzhagen IA (1996) Ultrastructure and quantification of synapses in the insect nervous system. *J Neurosci Methods* 69:59–73.
2. Meinertzhagen IA, O'Neil SD (1991) Synaptic organization of columnar elements in the lamina of the wild type in *Drosophila melanogaster*. *J Comp Neurol* 305:232–263.
3. Kosco MS, Loseth KJ, Crabo BG (1989) Development of the seminiferous tubules after neonatal hemicastration in the boar. *J Reprod Fertil* 87:1–11.
4. Blanco LN, Massaro GD, Massaro D (1989) Alveolar dimensions and number: developmental and hormonal regulation. *Am J Physiol* 257:L240–L247.

5. van Hateren JH (1984) Waveguide theory applied to optically measured angular sensitivities of fly photoreceptors. *J Comp Physiol A Neuroethol Sens Neural Behav Physiol* 154:761–771.
6. Warrant EJ, McIntyre PD (1993) Arthropod eye design and the physical limits to spatial resolving power. *Prog Neurobiol* 40:413–461.
7. Stavenga DG (2003) Angular and spectral sensitivity of fly photoreceptors. II. Dependence on facet lens F-number and rhabdomere type in *Drosophila*. *J Comp Physiol A Neuroethol Sens Neural Behav Physiol* 189:189–202.
8. Snyder AW, Miller WH (1972) Fly colour vision. *Vision Res* 12:1339–1396.
9. Horridge GA, Mimura K, Hardie RC (1976) Fly photoreceptors III. Angular sensitivity as a function of wavelength and limits of resolution. *Proc R Soc Lond B Biol Sci* 194: 151–177.
10. Warrant EJ, et al. (2004) Nocturnal vision and landmark orientation in a tropical halictid bee. *Curr Biol* 14:1309–1318.
11. Greiner B, Ribi WA, Warrant EJ (2004) Retinal and optical adaptations for nocturnal vision in the halictid bee *Megalopta genalis*. *Cell Tissue Res* 316:377–390.
12. Somanathan H, Warrant EJ, Borges RM, Wallén R, Kelber A (2009) Resolution and sensitivity of the eyes of the Asian honeybees *Apis florea*, *Apis cerana* and *Apis dorsata*. *J Exp Biol* 212:2448–2453.
13. Wijngaard W, Stavenga DG (1975) On optical crosstalk between fly rhabdomeres. *Biol Cybern* 18:61–67.
14. Juusola M, de Polavieja GG (2003) The rate of information transfer of naturalistic stimulation by graded potentials. *J Gen Physiol* 122:191–206.
15. Juusola M, Hardie RC (2001) Light adaptation in *Drosophila* photoreceptors: I. Response dynamics and signaling efficiency at 25 °C. *J Gen Physiol* 117:3–25.
16. Götz KG (1964) Optomotorische untersuchungen des visuellen systems einiger augenmutanten der fruchtfliege *Drosophila*. *Kybernetik* 2:77–92.
17. Hardie RC (1979) Electrophysiological analysis of fly retina. I: Comparative properties of R1-6 and R7 and 8. *J Comp Physiol A Neuroethol Sens Neural Behav Physiol* 129: 19–33.
18. Wilson M (1975) Angular sensitivity of light and dark adapted locust retinula cells. *J Comp Physiol* 97:323–328.
19. Hardie RC, Postma M (2008) Phototransduction in microvillar photoreceptors of *Drosophila* and other invertebrates. *The Senses: A Comprehensive Reference*, eds Albright TD, Masland R (Academic Press, San Diego), Vol 1, pp 77–130.
20. Weckström M, Hardie RC, Laughlin SB (1991) Voltage-activated potassium channels in blowfly photoreceptors and their role in light adaptation. *J Physiol* 440:635–657.
21. Faivre O, Juusola M (2008) Visual coding in locust photoreceptors. *PLoS ONE* 3:e2173.
22. Juusola M, Weckström M (1993) Band-pass filtering by voltage-dependent membrane in an insect photoreceptor. *Neurosci Lett* 154:84–88.
23. van Hateren JH (1997) Processing of natural time series of intensities by the visual system of the blowfly. *Vision Res* 37:3407–3416.
24. Shannon CE (1948) A mathematical theory of communication. *Bell Syst Tech J* 27: 379–423, 623–656.
25. de Polavieja GG, Harsch A, Kleppe I, Robinson HPC, Juusola M (2005) Stimulus history reliably shapes action potential waveforms of cortical neurons. *J Neurosci* 25: 5657–5665.
26. Zheng L, et al. (2006) Feedback network controls photoreceptor output at the layer of first visual synapses in *Drosophila*. *J Gen Physiol* 127:495–510.

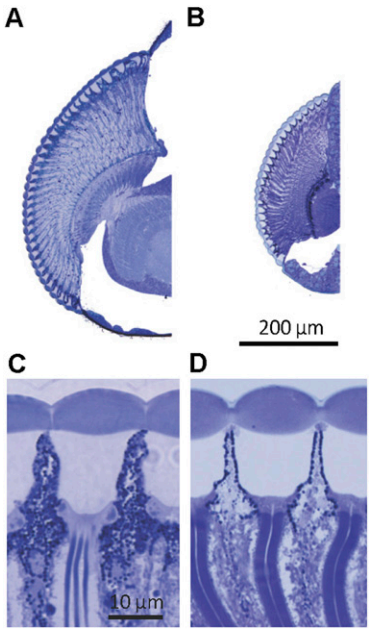

Fig. S1. Longitudinal and horizontal head sections. (*A* and *B*) Semithin (0.5-μm) longitudinal sections cut horizontally (antennae to neck) from *Coenosia* and *Drosophila*, respectively. (*C* and *D*) Longitudinal sections across the eye of female *Coenosia* and *Drosophila*, respectively. The higher concentration of screening pigments in *Coenosia* is evident. The lack of tapering of the rhabdomere diameter below the rhabdomere is also apparent, in particular in the *Drosophila* sample.

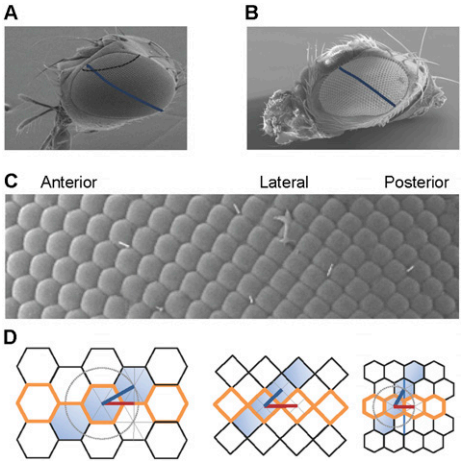

Fig. S2. Ommatidia shape and orientation. (*A* and *B*) The oblique cut crosses one ommatidia row in both *Coenosia* and *Drosophila*, respectively. (*C*) Pictures from a *Coenosia* eye showing the change in ommatidia size and shape across the horizontal axis. (*D*) Ommatidial arrangement diagrams representative of anterior, lateral, and posterior eye regions. Ommatidia that lay along the horizontal axis are outlined in orange. Ommatidia that lay along a diagonal section are filled with blue. Red lines and blue lines represent the distance measured from horizontal and oblique cuts, respectively, used to calculate $\Delta\varphi$. The horizontal cut induces bias by yielding smaller than real $\Delta\varphi$ at the front of the eye and larger than real $\Delta\varphi$ at the middle of the eye. The posterior part of the eye is measured appropriately by both cuts. Diagrams adapted from (1).

1. Stavenga DG (1975) The neural superposition eye and its optical demands. *J Comp Physiol* 102:297–304.

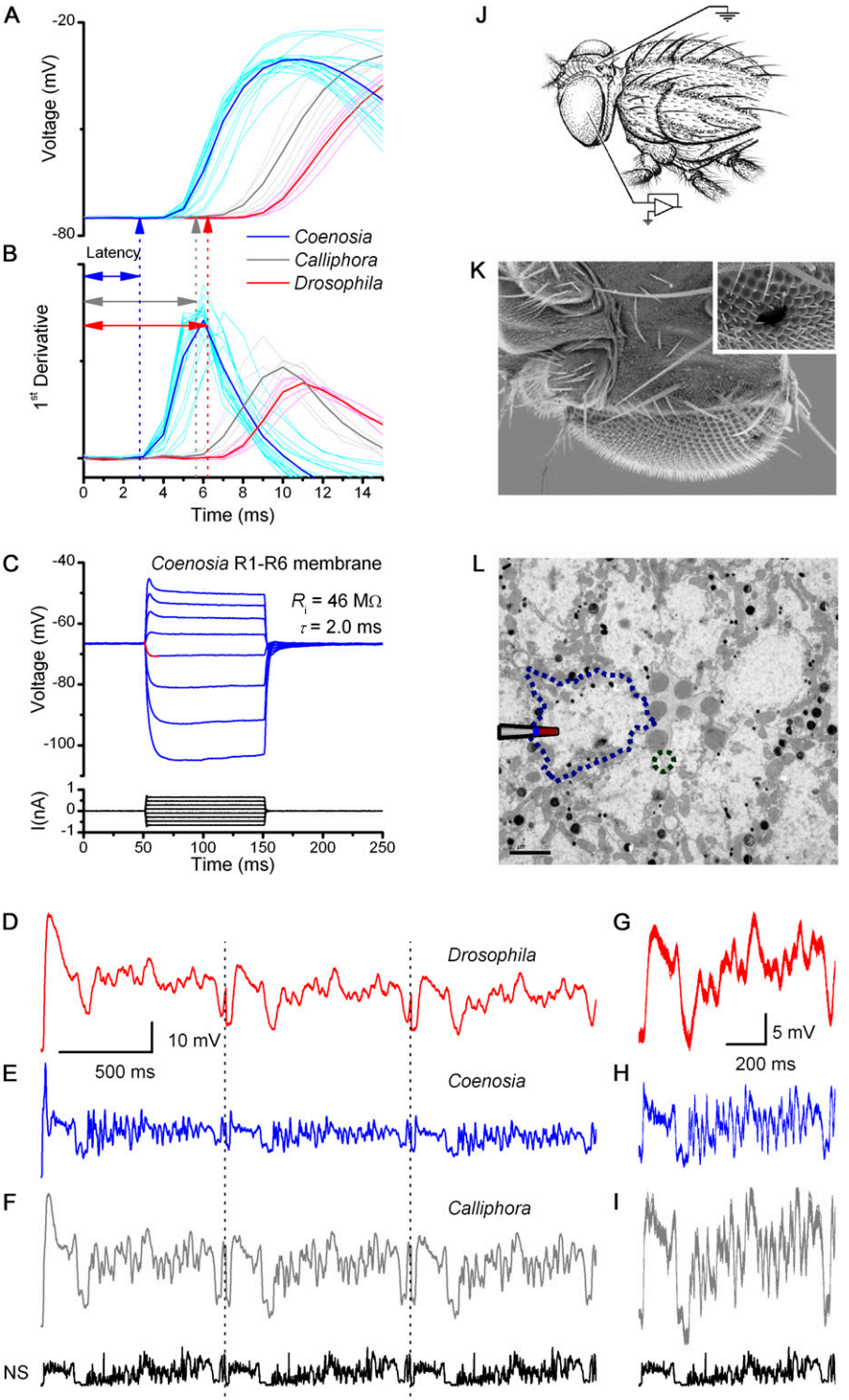

Fig. S3. Temporal photoreceptor properties of *Coenosia*, *Drosophila*, and *Calliphora*. (*A*) Voltage responses of five *Coenosia*, *Calliphora*, and *Drosophila* R1–R6 photoreceptors (thin traces) and their means (thick traces) to the same 10-ms light pulse (onset at zero) at 19 °C. (*B*) First derivatives of the individual responses (thin lines) and their means (thick traces). The vertical arrows (dotted lines) indicate when the first derivatives begin to rise on average, by producing a distinctive "up-notch" above the flat baseline. The horizontal arrows indicate the respective latencies. (*C*) Voltage responses (blue) of a *Coenosia* photoreceptor to injected current steps (gray) under dark conditions. Depolarizing current steps cause outward rectification and hyperpolarizing steps inward rectification of the membrane, suggesting activation of voltage-sensitive ion channels. The membrane time constant, τ, was estimated by fitting a single exponential to the smallest hyperpolarizing voltage response (red trace). (*D–F*) Voltage responses of *Drosophila*, *Coenosia*, and *Calliphora* R1–R6 photoreceptors to a repeated time series of natural light intensities (NS) at 19 °C. NS (black trace) causes rapid adaptation of the voltage responses. *Coenosia*'s response adapts the fastest and can encode fine details of the stimulus patterns from its onset onwards. Dotted lines section 1-s data chunks. (*G–I*) Forty consecutive responses to the 1-s-long NS at 19 °C are superimposed; after 10 s of stimulation. The voltage responses are highly reproducible but show distinctive differences between the species. These and similar responses were used for calculating the signal-to-noise ratio (Fig. 3*D*, main text) and the rate of information transfer (Fig. 3*E*, main

Legend continued on following page

text) of the photoreceptors. (*J*) The fly was fixed on a fly holder so that a reference electrode could be placed through the ocelli and a sharp conventional microelectrode could be inserted into the eye through a small opening in the cornea. Image reproduced from (1). (*K*) Scanning electron microscopy image of a fly head, in which a small opening has been cut in the cornea for in vivo intracellular recordings. *Inset:* Close up view of this "window." The size of the corneal window was typically four to six ommatidia (window width, 25–30 μm). (*L*) Scaled representations of the microelectrode tip (measured using scanning EM), used for intracellular recordings, and the transmission EM cross-section of a *Coenosia* ommatidium. (Scale bar, 2 μm.)

1. Krans J, Gilbert C, Hoy R (2006) Teaching insect retinal physiology with newly designed, inexpensive micromanipulators. *Adv Physiol Educ* 30:254–261.

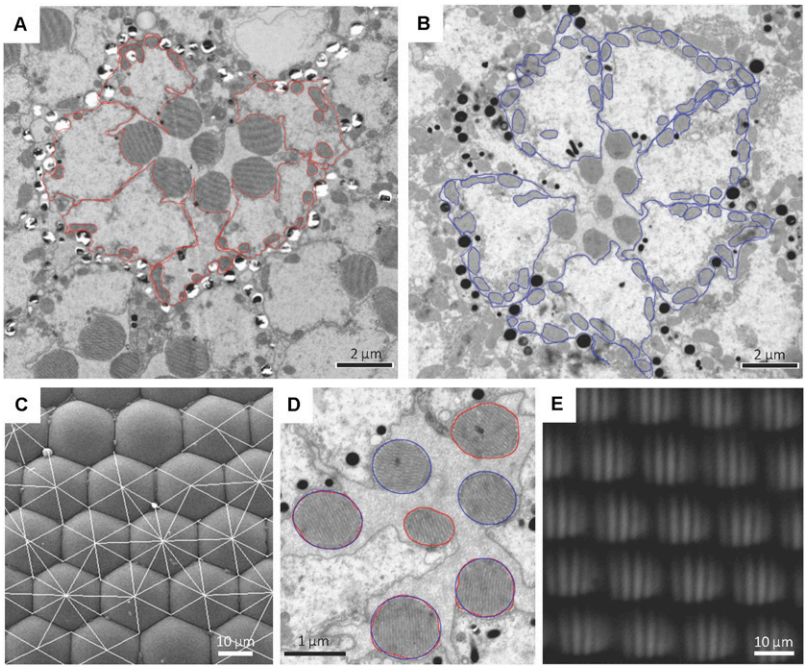

Fig. S4. Morphological measurements. (*A* and *B*) Representative profile areas measured from transmission EM (TEM) micrographs of (*A*) *Drosophila* and (*B*) *Coenosia*. Using ImageJ, the cytosol and mitochondria profiles from R1–R6 were traced by hand from 10 ommatidia (TEM micrographs). *Coenosia* had significantly more mitochondria profiles, and these were significantly larger than *Drosophila* (10.97 ± 0.27 and 4.08 ± 0.16 profiles, $P < 10^{-44}$; 2.26 ± 0.09 and 0.62 ± 0.03 μm^2, $P < 10^{-36}$, respectively). *Coenosia* mitochondria profiles also occupied a much greater proportion of photoreceptor cytosol than *Drosophila* (17.55% ± 0.39% and 8.22% ± 0.40% of the photoreceptor cytosol area, $P < 10^{-44}$, respectively). (*C*) Lens diameter was measured, from scanning EM micrographs, as the distance between the centers of neighboring lenses. (*D*) Rhabdomere diameter was measured from TEM micrographs. The rhabdomere area was selected by hand (red circles) and fitted with an ellipse (blue circles). (*E*) Focal plane of a *Coenosia* cornea viewing a grating.

Table S1. Eye parameters in *Coenosia* and *Drosophila*

Species	Lens (*n*)	D (μm)	Δφ (°)	Δρ (°)	*f* (μm)	$d_{maj\ -min,}$ R1–6 (μm)	$d_{maj\ -min,}$ R7 (μm)
Drosophila ♀	782 ± 17	16–17	3.2–8.0	8.23 ± 0.54	21.36	2.34–1.97	1.75–1.38
(*n*/≈sample no.)	2	1/12	2/33	11	1/14	1/12	1/12
Coenosia ♀	2,340 ± 21	14–20	2.3–7.8	2.88 ± 0.07	24.70 ± 1.15	1.10–0.97	0.83–0.68
(*n*/≈sample no.)	2	1/30	2/54	21	2/25	1/12	1/12
Coenosia ♂	1,851	13–17	2.3–6.2	2.69 ± 0.10	——	0.96–0.85	0.70–0.56
(*n*/≈sample no.)	1	1/14	2/53	4	——	1/12	1/12

Number of lenses, range of lens diameters (D), range of Interommatidial angles (Δφ), photoreceptor acceptance angle (Δρ, mean ± SEM), focal length (*f*, mean ± SEM). Mean distal major (d_{major}) and minor (d_{minor}) rhabdomere diameters obtained from photoreceptors in the lateral region of the eye. The number of individual flies and number of samples measured from each animal is shown (*n*/≈sample no.), except for Δρ, where *n* = number of cells.

Table S2. Angular diameter of the Airy disk

Species	$\Delta\rho_l$ front	$\Delta\rho_l$ rest
Drosophila ♀	1.60°	1.719°
Coenosia ♀	1.49°	1.833°
Coenosia ♂	1.73°	2.027°

Airy disk half-width in radians was calculated using $\Delta\rho_l = \lambda/D$ (1) / (degrees = radians × 180/π). The average values are estimated from data shown in Table S1, assuming λ = 0.5 μm.

1. Snyder AW (1977) Acuity of compound eyes: Physical limitations and design. *J Comp Physiol A Neuroethol Sens Neural Behav Physiol* 116:161–182.

Table S3. Distal major rhabdomere in the frontal and lateral areas of the eye

	Frontal		Lateral	
Species	R1–R6	R7	R1–R6	R7
Drosophila ♀	——	——	2.34 ± 0.02	1.75 ± 0.03
(*n*/≈sample no.)	——	——	1/12	1/12
Coenosia ♀	1.08 ± 0.02	0.91 ± 0.02	1.10 ± 0.01	0.83 ± 0.02
(*n*/≈sample no.)	1/13	1/13	1/12	1/12
Coenosia ♂	0.96 ± 0.02	0.85 ± 0.04	0.96 ± 0.01	0.70 ± 0.02
(*n*/≈sample no.)	1/12	1/12	1/12	1/12

Number of individual flies and number of samples measured from each animal is shown [*n*/≈sample no.; mean ± SEM (μm)].

Table S4. Cross-talk between photoreceptors

Species	Depth	*d* (μm)	*b* (μm)	*e* (μm)	*Cross-talk* (*e*/*b*) + 2
Drosophila ♀	Distal	2.15	1.075	0.10	2.09
Coenosia ♀	Distal	0.985	0.492	0.24	2.487
Coenosia ♂	Distal	0.905	0.452	0.235	2.519
Drosophila ♀	Waist	2.25	1.125	0.31	2.275
Coenosia ♀	Waist	0.88	0.44	0.858	3.95
Coenosia ♂	Waist	0.935	0.467	0.873	3.86

Relative rhabdomere diameter as a measure of cross-talk along the ommatidium. Rhabdomere diameter (*d*) calculated as the mean between d_{major} and d_{minor}. Rhabdomere radius *b* = *d*/2. Shortest length between boundary of neighboring rhabdomeres = *e*. Data shown from average R1–R6. For each level and genotype, *n* = the same as those reported for Table S1.

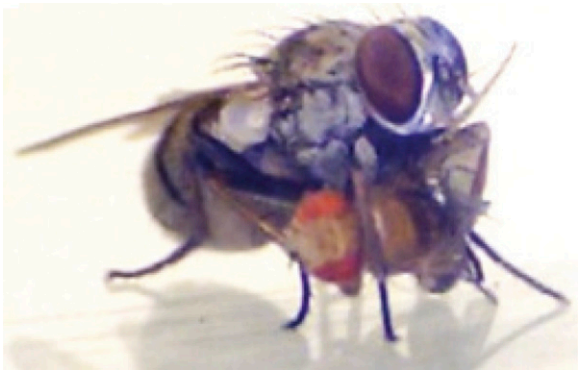

Movie S1. High-speed video of *Coenosia* prey capture. This movie shows a *Coenosia* specimen catching a *Drosophila* midflight, using an intercepting trajectory, filmed at 250 frames per second.

Movie S1